



BNL-91254-2010-BC

Zinc Transporter YiiP Escherichia coli

Dax Fu

Department of Biology, Brookhaven National Laboratory, Upton NY 11973

To be published in "Handbook of Metalloproteins"

March 2010

Biology Department
Brookhaven National Laboratory
P.O. Box 5000
Upton, NY 11973-5000
www.bnl.gov

Notice: This manuscript has been authored by employees of Brookhaven Science Associates, LLC under Contract No. DE-AC02-98CH10886 with the U.S. Department of Energy. The publisher by accepting the manuscript for publication acknowledges that the United States Government retains a non-exclusive, paid-up, irrevocable, world-wide license to publish or reproduce the published form of this manuscript, or allow others to do so, for United States Government purposes.

This preprint is intended for publication in a journal or proceedings. Since changes may be made before publication, it may not be cited or reproduced without the author's permission.

DISCLAIMER

This report was prepared as an account of work sponsored by an agency of the United States Government. Neither the United States Government nor any agency thereof, nor any of their employees, nor any of their contractors, subcontractors, or their employees, makes any warranty, express or implied, or assumes any legal liability or responsibility for the accuracy, completeness, or any third party's use or the results of such use of any information, apparatus, product, or process disclosed, or represents that its use would not infringe privately owned rights. Reference herein to any specific commercial product, process, or service by trade name, trademark, manufacturer, or otherwise, does not necessarily constitute or imply its endorsement, recommendation, or favoring by the United States Government or any agency thereof or its contractors or subcontractors. The views and opinions of authors expressed herein do not necessarily state or reflect those of the United States Government or any agency thereof.

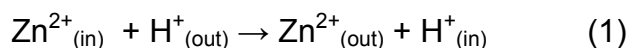
Zinc Transporter YiiP *Escherichia coli*

Dax Fu

Department of Biology, Brookhaven National Laboratory, Upton, NY 11973

FUNCTIONAL CLASS

Purified YiiP in the reconstituted proteoliposomes catalyzes a transmembrane zinc-for-proton exchange according to reaction scheme (1):



YiiP is a selective metal transporter for Zn^{2+} and Ca^{2+} [1]. *In vivo* transport data suggested that YiiP may function as a Fe^{2+} efflux transporter. Thus, YiiP also is named FieF for ferrous iron efflux [2].

OCCURRENCE

YiiP is an integral membrane protein found in the cytoplasmic membrane of *Escherichia coli* [3]. Transcription of chromosomal *yiiP* gene is inducible by Zn^{2+} and Fe^{2+} in a concentration dependent manner [2]. YiiP belongs to the protein family of cation diffusion facilitator (CDF) [4]. Members of the CDF family occur at all phylogenetic levels from bacteria to archaea and eukaryotes [5]. Most eukaryotic CDFs localize in various intracellular organelle membranes, such as vacuoles of plants and yeast [6, 7], and the Golgi of animals [8, 9].

BIOLOGICAL FUNCTION

CDFs are proton-driven metal antiporters [10-13] that catalyse the efflux of divalent transition metal ions, including Zn^{2+} , Co^{2+} , Fe^{2+} , Cd^{2+} , Ni^{2+} and Mn^{2+} from the cytoplasm to the extracellular medium or into intercellular membrane compartments [14-19]. Bacterial CDFs generally are involved in resistance to metal overexposure [20]. The functional role of YiiP is implicated by cell growth under metal stress conditions. A double deletion of *yiiP* and the

ferrous iron uptake regulator *fur* increased iron sensitivity, whereas an over-expression of *yiiP* restored iron tolerance, accompanied by a decrease in Fe^{2+} accumulation in the cells [2]. The observed YiiP-dependent phenotype suggested that YiiP is involved in iron detoxification *in vivo* [2]. However, a ^{55}Fe -uptake assay showed that YiiP catalyzed active uptake of Zn^{2+} , but not Fe^{2+} , into everted membrane vesicles in a proton-dependent manner [2]. *In vitro* transport assay for purified YiiP also indicated that YiiP transported Zn^{2+} and Cd^{2+} into reconstituted proteoliposomes encapsulated with a zinc-selective fluorescent indicator for monitoring zinc influx [1]. At present, whether YiiP transports Fe^{2+} *in vitro* has yet to be determined, because a reliable Fe^{2+} indicator for is still lacking. A second *E. coli* CDF protein, ZitB, confers zinc resistance in a zinc-sensitive *E. coli* strain [3]. Purified ZitB catalyzes a 1:1 stoichiometric zinc-for-proton exchange in reconstituted proteoliposomes [10]. Thus, ZitB likely is a zinc-specific efflux transporter *in vivo*. The zinc transport activity of ZitB is obligatorily coupled to proton antiport. Despite the name of cation diffusion facilitator, ZitB is a secondary active transporter that converts a downhill proton gradient to an uphill pumping of Zn^{2+} against its concentration gradient. Additional examples of bacterial CDFs are CzcD from *R. metallidurans* and CzrB from *Thermus thermophilus*. CzcD mediates Zn^{2+} , Co^{2+} and Cd^{2+} resistance [14] while heterologous expression of CzrB in *E. coli* increases resistance to Zn^{2+} and Cd^{2+} , but not Co^{2+} [21].

Yeast CDFs from *Saccharomyces cerevisiae* comprise five homologs. ZRC1 and COT1 transport cytosolic Zn^{2+} , Cd^{2+} and Co^{2+} into vacuoles for storages and detoxification [22, 23]. A third *S. cerevisiae* CDF, MSC2 is involved in zinc homeostasis of the nucleus and endoplasmic reticulum [24, 25]. The rest two CDFs, MFT1 and MFT2, are Fe^{2+} transporters located in the mitochondrial membrane [26]. Plant CDFs adopt a naming system of MTP for metal tolerance protein [27]. *Arabidopsis* contains twelve MTPs. They have different substrate specificities and affinities, and, exhibits specific cellular and subcellular expression [28]. For example, multiple MTPs are found in vacuolar membranes [5]. They are energized by a proton gradient to transport Zn^{2+} against its concentration gradient into the vacuole, thereby playing a crucial role in plant metal resistance [29]. In mammals, all characterized CDFs transport Zn^{2+} , and so these proteins are named zinc transporter (ZnT) [30]. Ten mammalian ZnT homologs (ZnT 1-10) form family 39 in the classification of solute carrier proteins (SLC39) [31]. Among them, ZnT-1 is a zinc homeostatic protein, transporting excess cytoplasmic zinc out of cells [30]. Emerging evidence suggests that ZnT-1 may be involved in crosstalk with cellular calcium homeostasis [32] and in regulation of a Ras-signalling pathway

[33]. ZnT1 is the only mammalian CDF found in the cytoplasmic membrane. All other ZnTs are localized intracellularly, shuttling Zn²⁺ into intracellular and secretory vesicles. For examples, ZnT3 is responsible for replenishing zinc-rich synaptic vesicles after zinc release as a co-neurotransmitter at glutamatergic synapses [34, 35]. ZnT5 functions as a zinc/proton antiporter for vesicular zinc sequestration into the trans-Golgi sub-compartment [13]. ZnT8 is exclusively expressed in pancreatic insulin-producing beta cells [36]. A genome-wide association study established an association between a single nucleotide polymorphism marker on the human *znT8* gene and genetic susceptibility to type-2 diabetes [37]. The phenotype of ZnT8-null transgenic mice showed that ZnT8 is required for assembling insulin into zinc-containing hexamers [38]. Taken together, mammalian CDFs seem more involved in cellular signaling and regulation than survival-dependent zinc homeostasis.

AMINO ACID SEQUENCE INFORMATION

Escherichia coli (stain 12), YiiP or FieF, 300 amino acids, translation of DNA sequence SWP P69380

PROTEIN PRODUCTION AND PURIFICATION

Recombinant *E. coli* expression was used for large-scale production of YiiP in an expression strain, BL21 (DE3) pLysS. The expression plasmid was constructed based on a commercial vector pET15b (Novagen) with an inserted YiiP sequence fused in frame to a thrombin proteolytic cleavage site, followed by a C-terminal six-histidine affinity tag. YiiP expression is under the control of a T7 *lac* promoter [39]. Since isopropyl- β -D-thiogalactoside (IPTG) induction of YiiP over-expression was highly toxic to cell growth, cells were first grown under catabolite repression of the *lac* operon by glucose, and then YiiP over-expression was induced by lactose which gradually took over glucose as the cells approached higher densities. At an optimal glucose-to-lactose ratio as described by Studier [40], the lactose-induced cell culture typically reached an optical density (OD₆₀₀) of 4-6 absorbance units, corresponding to a ~20-fold increase in cell mass over the IPTG-induction.

Purification of YiiP consists of membrane vesicle preparation, detergent solubilization, initial affinity purification and a final size-exclusion HPLC polish [41]. Cells were harvested and

lysed by passing through an ice-chilled microfluidizer press cell. The resulting membrane vesicles were collected by ultracentrifugation, and then solubilized using n-dodecyl- β -D-maltopyranoside (DDM) at a 1:5 detergent-to-cell (w/w) ratio in a buffer containing 100 mM NaCl, 20 mM HEPES, pH 7.5, 0.25 mM Tris(2-carboxyethyl) phosphine hydrochloride (TECP) and 20% w/v glycerol. The DDM-solubilized YiiP was less than 0.5% of the total protein. The detergent crude extract was first passed through a DEAE anion exchange column, and then YiiP-TB-His was immobilized to a Ni²⁺-NTA affinity column, washed free of contaminants at an elevated imidazole concentration. The low-abundance starting material necessitated a stringent wash, but an excessive wash could over-delipidate YiiP to cause protein denaturation. A delicate balance between protein purity and delipidation was adjusted based on readouts of two UV detectors that monitored the entire purification process. The purified YiiP-TB-His was eluted by 500 mM imidazole, which was removed immediately by desalting the protein sample. Finally, 1 mM CdCl₂ was added to metallate YiiP eluted from the desalting column. A typical YiiP yield was 30 mg per liter of lactose-induced cell culture.

Prior to the final size-exclusion HPLC purification, YiiP-TB-His was loaded to a dialysis cassettes for simultaneous dialysis and protein concentration using a bulk dialysis buffer (20 mM HEPES, pH 7.5, 100 mM NaCl, 20% w/v glycerol, 0.05% DDM, 0.5 mM TCEP) with the addition of 5% PEG 35,000. Thrombin was added into the dialysis cassette at a ratio of 1 unit per mg YiiP-TB-YiiP to cleave the C-terminal poly-histidine peptide. Concentrated YiiP, typically at a concentration of 15 mg/ml, was incubated briefly with 5mM EDTA before injected to a size exclusion column pre-equilibrated with a degassed mobile phase (20 mM Na-citrate, pH 5.5, 100 mM NaCl, 12.5% glycerol, 0.05% DDM, 0.32 mM TCEP). The HPLC-polished sample was collected, concentrated to 15~20 mg/ml, and then dialyzed against a buffer containing 100 mM NaCl, 10 mM Na-citrate, 0.05% (w/v) n-undecyl- β -D-maltoside (UDM), 20% (w/v) Glycerol and 0.5 mM TCEP, pH 5.5. DDM/UDM detergent exchange completed after a two-week dialysis at 4°C.

MOLECULAR CHARACTERIZATION

The proteolytic cleavage of the His-tag was conformed by MALDI-TOF mass spectrometry and by Western-blot analysis using an antibody specific to the poly-histidine peptide. YiiP could be concentrated up to 20-25 mg/ml without compromising its monodispersity, as

judged by dynamic light scattering measurement. The mono-modal scattering profile suggested that YiiP and its associated detergents and lipids formed a homogenous micellar species. Analytical size-exclusion HPLC showed that YiiP elutes as a major mono-disperse species with a retention time corresponding to an apparent molecular weight of 190 KDa. The oligomeric state of the purified YiiP in the detergent-lipid micelles was determined by simultaneous measurements of ultraviolet (UV) absorption, light-scattering (LS) and differential refractive index (RI) of the YiiP peak fraction [42]. This UV-LS-RI method gave absolute protein mass irrespective of the size, shape and lipid-detergent constituent of the mixed micelles. When YiiP was solubilized in four types of maltoside detergents, the protein mass distribution in the micelles was found within a narrow range matching the predicted mass of a YiiP dimer [43]. In contrast, the detergent-lipid masses in the YiiP micelles increased with the detergent chain-length. The subunit organization of YiiP in the lipid bilayer was visualized by electron microscopy of two-dimensional YiiP crystals in negative stain. A projection structure calculated from measurable optical diffractions to 25-Å revealed a dumbbell-shaped homodimer profile [43]. The dimeric assembly of YiiP in the native cytoplasmic membrane was confirmed by crosslinking analysis [43]. Therefore, the detergent solubilized YiiP seems to retain its native dimeric assembly.

Metal binding to the purified YiiP was characterized by isothermal titration calorimetric (ITC) analysis [41]. Zn^{2+} titrations exhibited a characteristic exothermic-to-endothermic transition, suggesting the presence of at least two sets of independent Zn^{2+} binding sites. The zinc titration data indicated a binding stoichiometry of 2.34 Zn^{2+} equivalents per YiiP monomer, but binding parameters was not attainable because the multiphase of the Zn^{2+} binding isotherm precluded a reliable parameter fitting. Cd^{2+} titrations yielded a single exothermic isotherm that could be fitted to a two-site model with $K_{a1}=8.70\pm 0.45 \mu M^{-1}$, $n_1= 1.2\pm 0.1$, $\Delta H_1= -6.5\pm 0.1$ kcal/mol; $K_{a2}=0.30\pm 0.05 \mu M^{-1}$, $n_2= 0.84\pm 0.05$, $\Delta H_2= -6.1\pm 0.7$ kcal/mol. A Zn^{2+}/Cd^{2+} competition assay showed that Cd^{2+} binding abolished the exothermic zinc heat component, but had little effect on the endothermic Zn^{2+} binding. It appeared that the two Cd^{2+} binding sites in YiiP both overlap with the exothermic Zn^{2+} binding sites. The enthalpy change of Cd^{2+} binding to a common binding site was found linearly related to the ionization enthalpy of the pH buffer with a slope corresponding to the release of 1.23 H^+ upon each Cd^{2+} binding [41].

ACTIVITY TEST

YiiP with only 300 residues alone can transport zinc in response to cytoplasmic zinc binding. Activity was assayed using HPLC-purified YiiP reconstituted into proteoliposomes that were prepared from *E. coli* polar lipids (Avanti). Zinc influx was elicited by rapidly mixing proteoliposomes with zinc, and monitored using a zinc selective fluorescent indicator FluoZin-1 encapsulated inside the proteoliposomes [10]. The specific activity of YiiP was estimated based on a calibration of the FluoZin-1 fluorescence signal to the actual zinc flux, giving a turnover number of 12 s^{-1} for the purified YiiP in reconstituted proteoliposomes.

X-RAT STRUCTURE

Crystallization

YiiP crystals were grown by the hanging drop vapour diffusion method at 20°C by mixing equal volumes of protein (10 mg/ml) with a reservoir solution containing 100 mM Na-citrate (pH 6.0), 5 mM ZnSO₄, 3 mM Fos-Choline-12, 100 mM NaCl, 200 mM (NH₄)₂SO₄, 10% (v/v) PEG400, 15-20% (w/v) PEG2000, 4% (w/v) benzamidine, 10% (w/v) glycerol and 4% (v/v) 1,3-propanediol. Crystals grew to a full size of about 150 μm x 50 μm x 20 μm within 2 months. The lattice is orthorhombic, space group P222₁ with unit cell dimensions $a=106.7 \text{ \AA}$, $b=110.8 \text{ \AA}$, and $c=130.7 \text{ \AA}$. Each asymmetric unit contains two YiiP protomers that belong to two distinct physiological homodimers. YiiP crystals exhibited a large variation in x-ray diffraction quality. Only a small fraction of YiiP crystals diffracted to 3.8 Å. The first YiiP structure was solved by multiple isomorphous replacement and anomalous scattering phasing using diffraction datasets collected from native and twelve heavy atom derivative crystals [44]. Mercury derivatization of the YiiP crystals yielded a second crystal form. The space group is P2₁ with $a=105.7 \text{ \AA}$, $b=130.7 \text{ \AA}$, $c=115.8 \text{ \AA}$, $\beta=93.3^\circ$. Each asymmetric unit contains four copies of YiiP protomers that form two physiological homodimers. The best P2₁ crystals diffracted to 2.9 Å. A refined YiiP structure was obtained at this resolution by single isomorphous replacement and anomalous scattering phasing aided by molecular replacement [45].

Overall description of the structure

The YiiP crystal structure revealed a Y-shaped dimeric architecture arranged around a two-fold axis oriented perpendicular to the membrane plane [44]. Each protomer comprises an N-

terminal transmembrane domain (TMD) followed by a C-terminal domain (CTD) that protrudes into the cytoplasm (Figure. 1). Two CTDs of a YiiP homodimer juxtapose each other in parallel to form the major dimerization contact. At the CTD and TMD juncture, highly conserved inter-protomer salt bridges [45] and hydrophobic contacts form another dimerization contact, from which two TMDs swing outward and plunge into the membrane. The resulting Y-shaped architecture dramatically differs from most cylindrically-shaped membrane proteins. The hydrophobic mismatch between the TMD surface and the lipids in the space between two TMDs would deform the lipid bilayer, which in turn would directly impact YiiP conformations. How much of the native conformation of YiiP is preserved in the crystal structure has yet to be evaluated.

Each TMD of YiiP contains six TMs, fully consistent with earlier topology mapping data, showing that the YiiP polypeptide traverses the cytoplasmic membrane six times with both the N- and C-terminus in the cytoplasm [1]. The packing of transmembrane helices (TMs) in TMD falls into the “knobs-into-holes” type of helix-Interdigitation with standard TM crossing angles. A lack of the helix-breaking Pro residue in the middle of any TM suggests rather limited flexibility in each TM. The overall organization of TM1–6 can be grouped into two subdomains: TM1, TM2, TM4 and TM5 form a compact four-helix bundle, whereas the remaining TM3 and TM6 crossover in an antiparallel configuration outside the bundle (Figure 2). TM3 is tilted away from TM2; consequently, one side of the TM3-TM6 pair embraces TM5 at one corner of the rectangle-shaped four-helix bundle, whereas the other side projects highly conserved hydrophobic residues into the TMD-TMD interface to seal the bottom of the V-shaped void [44]. The orientation of the TM3-TM6 pairs is stabilized by four interlocked salt bridges formed between K77 of TM3 and D207 from a short loop that connects TM6 to the CTD [45]. These highly conserved charged residues are arranged in a circular fashion to form a $(K77-D207)_2$ charge interlock that bundles together the cytoplasmic ends of two TM3-TM6 pairs at the dimer interface as well as at the domain interface between TMD and CTD.

Among the six TMs, the length of TM5 is conspicuously short, accounting for four helical turns from residue Q145 to M159. This short helix is largely sequestered in the centre of the six-helix bundle, thereby giving rise to one extracellular and one intracellular cavity on either side of the membrane (Figure 3). The extracellular cavity is accessible from the bulk solvent and exposed to the membrane outer leaflet. This cavity spans nearly half of the membrane thickness, and is lined with negatively charged residues that provide a favourable

electrostatic environment for a bound Zn^{2+} ion near the bottom of the cavity. The intracellular cavity is surrounded by the cytoplasmic ends of TM3, TM5 and TM6. The two cavities from different sides of the membrane point toward each other within the membrane, but no connecting channel exists between them. The hydrophobic seal between the two cavities is stabilized by two highly conserved salt bridges, E79-R11 and E200-R148 in the interior of the intracellular cavity. They anchor the TM3-TM6 pair to the four-helix bundle in a manner reminiscent of the interhelical salt bridges in the rhodopsin-family GPCR [46-48] and LacY [49], wherein the salt bridges act as molecular switches to lock protein conformations that can be released by substrate binding [50-52].

In each TMD, TM1 to TM6 are linked together by three extracellular loops, denoted as EL1 to EL3, and two intracellular loops, IL1 and IL2 (Figure. 2). An additional intracellular loop, IL3, connects TM6 to the CTD. IL1 extends toward the dimer interface and forms a dimerization contact with IL3 from the neighbouring subunit [44]. IL2 is situated at the entrance to the intracellular cavity. In YiiP, it connects TM4 and TM5 with only four residues from position 141 to 144. Many CDF members contain a more extended IL2, commonly referred to the histidine-rich loop [4]. Functional studies showed that deletion of this histidine-rich Loop of AtMTP1 stimulates Zn^{2+} transport activity [11], and the loss of the histidine-rich loop in TgMTP1 confers increased Ni^{2+} specificity [19]. These results suggest that the histidine-rich loop plays a role in regulating transport activity and selectivity. On the extracellular membrane surface, all three extracellular loops adopt extended conformations with full exposure to solvent. However, EL3 in the membrane-bound YiiP may adopt a different conformation that protects a S171C mutation in EL3 from thiol-specific labelling [1]. The functional relevance of the extended EL3 conformations has yet to be evaluated.

The C-terminal domain (CTD) of each protomer adopts an open α - β fold with two alpha helices (H1-2) on one side of the domain and a three-stranded mixed β -sheet (S1-3) on the other side (Figure 2). S1 is antiparallel to S2, joined together by a hairpin loop. S2, H2 and S3 form a right-handed $\beta\alpha\beta$ motif with the two β -strands and the connecting α -helix all aligned approximately in parallel. The CTD exhibits an overall structural similarity with the copper metallochaperone Hah1 [53], although there is no sequence homology between YiiP and Hah1. The fold of CTD places it into the same structural category as a possible Zn^{2+} receiving domain [54]. The second important feature of CDT is represented by a charge-rich

CTD-CTD interface stretching from the (K77-D207)₂ charge interlock at the TMD-CTD juncture to the tip of the CTD, which extends 30 Å into the cytoplasm [45]. The electrostatic repulsion between two CTDs is neutralized by zinc binding at the CTD-CTD interface (see below).

Zinc sites

The crystal structure of YiiP was determined in complex with its metal substrate. Four ligated zinc ions (Z1-Z4) were found in each protomer. Z1-Z4, together with protein ligands and water molecules that participate in their first coordination shells constitute three distinct Zn²⁺ binding sites, A, B, and C. The multi-site operation in YiiP does not fall into the single binding-site, alternating-access paradigm ascribed to LacY, GlpT, NhaA, LeuT and many other secondary membrane transporters [49, 55-57]. Rather, recent progress in structural analyses of Ca²⁺, Mg²⁺ and Zn²⁺ transporters [58-64] has begun to coalesce into a distinct paradigm based on a common two modular architecture, corresponding to two interweaving processes, *viz.*, the signal transduction that is triggered by cation binding to the cytoplasmic sensing domain, and, the responding cation transport events in the transmembrane domain (TMD) [65]. The YiiP crystal structure reveals distinct coordination environments of three Zn²⁺ binding sites that are tailored to achieve two distinct functions: selective zinc transport and allosteric regulation of the Zn²⁺ transport [45].

Z1 in SA is tetra-coordinated by highly conserved D45, D49 from TM2, and H153, D157 from TM5 (Figure 4). They form a coordination system with four ligand groups (Asp45 O δ 1, Asp49 O δ 2, His153 N ϵ 2 and Asp157 O δ 2) positioned at the vertexes of a nearly ideal tetrahedron [45]. Tetrahedral coordination is preferred for Zn²⁺ and Cd²⁺, as opposed to the octahedral coordination that is preferred for most other divalent cations [66]. The observed tetrahedral coordination in crystal structure is consistent with an earlier finding that SA can bind Zn²⁺ and Cd²⁺, but not Fe²⁺, Mg²⁺, Ca²⁺, Mn²⁺, Co²⁺ or Ni²⁺[1]. SA exhibits three features well suited to rapid on-off switching of zinc coordination as expected for a zinc transporter. First, all ligating residues in SA are completely unconstrained, thus no making or breaking of outer shell interactions is needed for Zn²⁺ binding and release during a transport cycle [67]. Second, each of the three Asp-carboxylates in SA is mono-coordinated, leaving an unligated carboxylate oxygen ligand free of outer-shell interaction. These “dangling” carboxylate oxygens potentially can be rearranged to enter the coordination shell, resulting in a highly

adaptable inner-shell arrangement with varied coordination geometries and numbers [68]. The resultant conformational flexibility of SA may contribute to a rapid Zn^{2+} turnover rate of YiiP, which is several orders of magnitudes faster than Zn^{2+} exchange rates for typical zinc metalloproteins. Third, SA is confined exclusively between TM2 and TM5. A small inter-helix shift between TM2 and TM5 can lead to a large readjustment of the zinc-coordination geometry either in favour of zinc binding or release, thereby allowing for allosteric regulation of zinc coordination through protein conformational changes [45].

Z2 in SB is 5-coordinated by two His-imidazoles, a bidentate Asp-carboxylate and a water molecule that takes up the fifth coordinate. The presence of a coordinated water molecule is characteristic of zinc coordination in hydrolytic zinc enzymes [69], but its functional role in a membrane transporter is not clear. All Z2 ligating residues are located within an intracellular loop (IL1) that connects TM2 and TM3. The IL1 conformation is stabilized by an intra-loop hydrogen bond between H75 N δ 1 and mainchain carbonyl of P66, while another outer shell hydrogen bond is made between H71 N ϵ 2 and Q203 O ϵ 1 from TM6 of the neighbouring subunit. These outer shell interactions stabilize dimeric association and constrain relative TM orientation near the cytoplasmic membrane surface.

Z3 and Z4 are 3.8 Å apart in the binuclear SC, located at the interface of two associated C-terminal domains (CTDs). The carboxylate group of conserved D285 bridges Z3 and Z4. Additional coordination residues to Z3 are H232 and H248, and those to Z4 are H283 and H261 from the neighbouring subunit. These residues are tucked into the dimer interface in a cleft capped by two ligating water molecules. The positive charges on the two coordinated Zn^{2+} in SC balance the strong electronegativity of two opposing CTD surfaces, thereby stabilizing CTD-CTD dimerization [45]. Another important feature of SC is its extensive outer shell constraints. H232, H248 and H261 each donates a hydrogen bond to a carboxylate provided by E250, D233 and D265, respectively. H283, on the other hand, donates a hydrogen bond to Q284 of the neighbouring subunit. Each of those outer shell residues can potentially accept an additional hydrogen bond from a neighbouring protein donor or a water molecule to further expend the outer shell interactions at the dimer interface between two CTDs. These outer-shell interactions allows effective coupling of Zn^{2+} coordination at CTD-CTD interface to inter-CTD conformational changes [45].

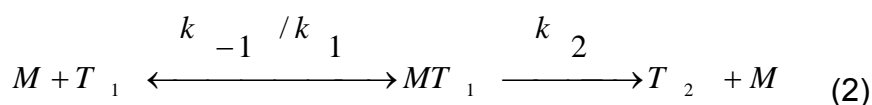
FUNCTIONAL ASPECTS

Roles of three zinc sites

The functional roles of SA, SB and SC were characterized by mutation-function analysis. SA is located at the bottom of the extracellular cavity (Figure 3). A D49A or D157A mutation to SA disrupted metal binding and completely abolished transport activity, indicating that SA is the active-site for zinc transport [1, 70]. SA was found highly selective for Zn^{2+} and Cd^{2+} , but not for Fe^{2+} and other divalent cations [1]. SB is localized to the TM2-TM3 connecting loop on the cytoplasmic membrane surface. None of these coordinating residues is conserved. Disruption of zinc binding to SB by a D68A had little effect on zinc transport activity, suggesting that SB is not involved in zinc transport. SC is located at the CTD-CTD interface. Binuclear zinc binding to site-C stabilizes a highly negatively charged CTD-CTD interface through extensive outer-shell constraints. A H232A mutation abolished zinc binding to site-C, impaired a zinc-induced inter-CTD conformational change, allosterically affected zinc binding to a reporter cysteine in SA, and reduced the rate of zinc transport [45]. These data collectively suggested that SC serves as a zinc sensor to gauge the cytoplasmic zinc concentration while extensive outer shell interactions around SC enable a tight coupling of binuclear zinc coordination to inter-CTD conformational changes [45]. The crystal structure of YiiP suggests that the release of zinc from the CTD-CTD interface would entail unbalanced electronegativity, causing two juxtaposed CTDs to swing apart by electrostatic repulsion in a hinge-like motion pivoting around the $(K77-D207)_2$ charge-interlock.

Transport kinetics

Stopped-flow measurements of transmembrane zinc flux through purified YiiP were performed using reconstituted proteoliposomes encapsulated with a fluorescent zinc indicator, FluoZinc-1 [1]. The rate of the fluorescence rise k_{obs} increased in a hyperbolic manner as a function of the Zn^{2+} concentration. This kinetic behaviour is consistent with a two-step process [10] shown in the following scheme:



where T_1 and T_2 are different conformational states of YiiP, and M is the metal substrate. The first step is a rapid equilibrium with a binding constant k_{-1}/k_1 , followed by a rate-limiting conformational transition from T_1 to T_2 with a rate constant k_2 . The relationship among k_1 , k_{-1} and k_2 is defined by $K_m=(k_2+k_{-1})/k_1$. Application of the steady-state condition to the MT_1 species gives equation (3)

$$1/K_{obs}=1/k_3+(K_m/k_3)/[M] \quad (3)$$

Linear regression of $1/K_{obs}$ as a function of $1/[M]$ yielded a k_3 value of $34\pm 5 \text{ s}^{-1}$ and a K_m value of $310\pm 32 \text{ }\mu\text{M}$.

Mechanism

Zn^{2+} is a small ion (radius 0.65 \AA) with a fixed valance of two. The high charge density on this ion rivals that of Mg^{2+} , but Zn^{2+} has a much higher electron affinity. Consequently, zinc exchange from its ligand groups often occurs over a period of hours [66]. It is a significant challenge to move the densely charged Zn^{2+} across the membrane barrier and move it rapidly on a 30-millisecond timescale. The most obvious distinction of the YiiP structure is represented by a pair of cavities that extend into the lipid bilayer from opposite membrane surfaces. The openings of both cavities measures more than 15 \AA in diameter, posing no obstruction for solvent exchange with the bulk solution. Neither the cavity interiors contain narrow regions to restrict free diffusion of Zn^{2+} in a fully hydrated form. Thus, water of hydration would significantly reduce the free energy barrier to Zn^{2+} diffusion in the low dielectric environments of the inner membrane [71]. From an energetic standpoint, zinc transport would occur at a breaching point within a hydrophobic seal that narrowly separates the two cavities. The YiiP crystal structure suggests that highly conserved salt bridges in the intracellular cavity contribute to stabilizing the hydrophobic seal.

Another essential component of the zinc transport reaction is the proton antiport. In the absence of proton, zinc transport would arrest despite an imposing Zn^{2+} gradient. This obligatory proton-coupled zinc transport mechanism is ascribed to all the CDF members characterized thus far [2, 10, 12, 13]. For example, zinc transport by ZitB is coupled obligatorily with proton antiport [10]. The pK_a of the ZitB transport activity is 7.7, which is

within the physiological pH range of the bacterial cytoplasm [72]. Since Cd^{2+} binding to YiiP was shown to displace proton with a ~1:1 stoichiometry [41], we propose a minimal three-step $\text{Zn}^{2+}/\text{H}^+$ antiport model as depicted in Figure 7. In step-1, zinc binding from the cytoplasm deprotonates an Arg residue engaged in a salt bridge in the intracellular cavity, and a proton from the periplasm releases a ligated-zinc from the active-site in the extracellular cavity by a $\text{zinc}^{2+}/\text{H}^+$ exchange. During step-2, YiiP undergoes a conformational change to open an inter-cavity 'channel'. The Arg-ligated zinc ion passes through the 'channel' to enter the active-site where it deprotonates one of the tetrahedral coordinating residues. The proton released from the active-site simultaneously moves across the inter-cavity 'channel' to re-protonates the Arg residue. In step-3, YiiP closes the inter-cavity 'channel' and re-establishes the salt-bridge to complete the $\text{Zn}^{2+}/\text{H}^+$ antiport cycle. Arg residues seem well suited for a role in $\text{Zn}^{2+}/\text{H}^+$ antiport. Arg residues relay proton transfer in the centre of a proton transport pathway in bacteriorhodopsin [73]. The unprotonated Arg guanidine group also can act as a metal ligand for zinc binding [74].

Regulation of activity

Differing from many membrane transporters that contain only one substrate binding-site, YiiP has three substrate binding-sites in each protomer: an active-site in TMD, and two additional zinc sites that are accessible to zinc binding from the cytoplasm. The multi-site operation of YiiP does not fall into the single binding-site, alternating-access mechanism ascribed to LacY, GlpT, NhaA, LeuT and many other secondary membrane transporters [49, 55-57]. Rather, recent progress in structural analyses of Ca^{2+} , Mg^{2+} and Zn^{2+} transporters [58-63] has begun to coalesce into a distinct paradigm based on a common two modular architecture, corresponding to two interweaving processes, *viz.*, a signal transduction that is triggered by cation binding to the cytoplasmic sensing domain, and, a responding cation transport event in the transmembrane domain [65]. The zinc-regulated, zinc-transport mechanism allows YiiP to directly respond to changes in cytoplasmic zinc concentrations and modulate its efflux activity around a homeostatic set-point. The crystal structure of YiiP suggests that cytoplasmic zinc binding would trigger a hinge-like inter-CTD conformational change pivoting around the $(\text{K77-D207})_2$ charge-interlock (Figure 8). This charge interlock is strategically situated at the CTD-TMD interface, well positioned to transmit inter-CTD conformational changes to TMD, wherein the charge interlock also stabilizes the orientation of the TM3-TM6 pair, which is linked sterically to the TM5-TM2 orientation in association with

coordination geometry of SA. Therefore, SC of CTD, the charger-interlock at the CTD-TMD interface, and SA of TMD define a regulatory pathway for allosteric regulation of zinc transport activity by cytoplasmic zinc binding. The charge interlock is among the most conserved structural elements in YiiP, suggesting a common allosteric mechanism for all CDF family members. A single R325W mutation in ZnT8 is represented in almost 25% of the global population at risk of developing type-2 diabetes [37]. Homology modeling of ZnT-8 localized the R325W mutation to the CTD interface. This mutation is more than 50-Å away from SA, thus unlikely has a direct effect on the active site for zinc transport. Rather, R325W may impair the allosteric pathway that transmits the activation signal of cytoplasmic zinc binding to the distant active-site in ZnT-8 [45].

Comparison with related structures

The CTD of YiiP is essentially identical to the C-terminal cytoplasmic domain of the Zn²⁺/Cd²⁺ efflux transporter CzrB from *Thermus thermophilus*. A ~100 amino acid soluble fragment of CzrB was crystallized with and without zinc. The crystal structures were solved to 1.7 Å for the apo form and 1.8 Å for the zinc-bound form [75]. Both structures reveal a dimeric association between two protomers. C α -trace superposition of a CTD of YiiP (residues 207-290) with one CzrB fragment (residues 200-288) either in apo- or zinc-bound form (PDB codes: 3BYP, 3BYR) yielded a RMSD less than 1.2-Å for 78 common C α atoms among three proteins [45]. However, despite the overall structural similarity among CTD protomers, the conformation of the dimeric CzrB fragment changes dramatically upon zinc binding. The two protomers are snapped together by zinc binding in a manner similar to dimeric CTD association in the fully length YiiP structure. In the apo-form, the two protomers seem to undergo a hinge-like *en bloc* motion, opening up the dimer interface at one end of the molecule that is expected to interact with TMD in the full length CzrB. In YiiP, a highly conserved charge interlock stabilizes CDT-CTD dimeric association at the CTD-TMD juncture. This charge interlock is missing in the CzrB fragment, thus raising the question as to the functional relevance of the observed conformational change. Each protomer of the CzrB fragment is associated with four zinc ions (Z1-4). The first three were found at or close to the interface between two protomers. They are likely present *in vivo*, but Z4 only exists in the crystal lattice. Z1 and Z3 are tetrahedrally coordinated whereas Z2 is hexacoordinated with classic octahedral geometry. It is noted that Z1 and Z2 are 4.9 Å apart, homologous with the two coordinated zinc ions in the binuclear zinc site (SC) of YiiP.

The CTD of YiiP shares a striking structural similarity to metallochaperones, a class of metal binding proteins involved in intracellular metal trafficking [76]. Metallochaperones deliver metal ions to specific target proteins, which also contain a metallochaperone-like domain that serves as the metal receiving module for interactions with a metallochaperone donor [77]. Both donor and acceptor proteins are characterized by a CxxC metal binding sequence [78]. The intermolecular metal transfer occurs by docking of the chaperone and target proteins to form a metal-bridged heterodimer complex in which the metal ion is ligated simultaneously by two CxxC motifs in close proximity at the protein interface [53]. In human, the well-characterized metallochaperone-target pairs are metallochaperone Hah1 and its targets, ATP7A and ATP7B [79]. Both proteins are metal-transporting P-type ATPases involved in intracellular copper homeostasis [80]. Mutations in the two Cu(I)-ATPase genes cause Menkes syndrome and Wilson's disease [81]. Each of the Menkes and Wilson disease proteins contains six metallochaperone-like domains, all of which can bind a single Cu(I) [82], but not all of them can accept copper from the Hah1 donor [83, 84]. In yeast, the prototypical metallochaperone-target pair is the copper chaperone Atx1 and the corresponding Cu(I)-transporting ATPase, Ccc2 [85]. In bacteria, The Cu-chaperone, CopZ delivers Cu(I) to the corresponding Cu(I)-ATPase, CopA [86]. At present, a zinc-specific metallochaperone has yet to be identified. Nevertheless, a zinc-transporting ATPase from *E. coli*, ZnTA, contains an N-terminal metallochaperone-like domain [87]. The CxxC metal binding motif of ZnTA likely is involved in Zn²⁺ transfer [88].

The crystal structure of Cd²⁺-Hah1 complex revealed Cd²⁺ coordination by two CXXC motifs at the interface of a Hah1-Cd²⁺-Hah1 homodimer [53]. The structure of a Hah1 protomer is built up from two βαβ motifs linked together by a hairpin loop corresponding to the S1-S2 connection in the CTD of YiiP (Figure 2). To a first approximation, the topologies of the Hha1 βαβ-βαβ fold and the αβ-βαβ fold in the CTD of YiiP are identical except that the first β-strand in Hah1 is missing in YiiP. The structural core of the CTD from H1 to H2 can be superimposed onto the equivalent portion in Hah1 (αβ-βα) with a root mean square deviation of 1.8 Å for 42 common Ca positions [44]. The last β-strand in the CTD diverges significantly from that of Hah1 because the missing first strand is required to hold the last strand in the Hha1 position through an antiparallel packing interaction. Despite the overall structural similarity, CDT of YiiP neither has a CxxC metal binding sequence, nor an overall sequence

homology with Hah1. Thus, their structural similarity appears to arise independently of each other through convergent evolution at the structural level.

A model of a metallochaperone-YiiP protein complex is proposed based on the crystal structures of YiiP and Hha1 homodimers. Superposition of a Hha1 and a CTD allowed placement of a second Hha1 structure onto the putative docking position [44]. As shown in Figure 9, the docked metallochaperone rests on the CTD surface and fits snugly between TMD and CDT with a putative Zn^{2+} transfer site positioned right at the entrance to the intracellular cavity. In this model, the putative zinc-metallochaperone would directly deliver its zinc cargo to the intracellular cavity of YiiP for zinc translocation across the membrane. The docking of the metallochaperone blocks much of the solvent accessibility to the intracellular cavity, thereby preventing back flow of Zn^{2+} into the cytoplasm. The histidine-rich loop found in many CDF homologs is located in close proximity to the Zn^{2+} transfer site, thus may play an important role in mediating the Zn^{2+} delivery process. According to this model, the metallochaperone-YiiP docking is only possible when two CTDs are clamped together by binuclear zinc binding to SC at the CTD interface. Therefore, cytoplasmic Zn^{2+} binding assures an inter-domain space between CTD and TMD for docking of a zinc-loaded metallochaperone.

ACKNOWLEDGEMENTS

This work is supported by the National Institute of Health and Office of Basic Energy Sciences, Department of Energy. BNL is managed by Brookhaven Science Associates for the Department of Energy.

REFERENCES

- 1 **Wei, Y. and Fu, D.** Selective metal binding to a membrane-embedded aspartate in the Escherichia coli metal transporter YiiP (FieF). *J Biol Chem.*, 2005, **280**(40), 33716-33724.
- 2 **Grass, G., Otto, M., Fricke, B., Haney, C.J., Rensing, C., Nies, D.H. and Munkelt, D.** FieF (YiiP) from Escherichia coli mediates decreased cellular accumulation of iron and relieves iron stress. *Arch Microbiol.*, 2005, **183**(1), 9-18.

- 3 **Grass, G., Fan, B., Rosen, B.P., Franke, S., Nies, D.H. and Rensing, C.** ZitB (YbgR), a member of the cation diffusion facilitator family, is an additional zinc transporter in *Escherichia coli*. *J Bacteriol.*, 2001, **183**(15), 4664-4667.
- 4 **Paulsen, I. and Saier, M.J.** A novel family of ubiquitous heavy metal ion transport proteins. *Journal of Membrane Biology*, 1997, **156**(2), 99-103.
- 5 **Montanini, B., Blaudez, D., Jeandroz, S., Sanders, D. and Chalot, M.** Phylogenetic and functional analysis of the Cation Diffusion Facilitator (CDF) family: improved signature and prediction of substrate specificity. *BMC Genomics*, 2007, **8**, 107.
- 6 **Eide, D.J.** Zinc transporters and the cellular trafficking of zinc. *Biochim Biophys Acta.*, 2006, **1763**(7), 711-722. .
- 7 **Hall, J.L. and Williams, L.E.** Transition metal transporters in plants. *J Exp Bot*, 2003, **54**(393), 2601-2613.
- 8 **Lichten, L.A. and Cousins, R.J.** Mammalian zinc transporters: nutritional and physiologic regulation. *Annu Rev Nutr*, 2009, **29**, 153-176.
- 9 **Kambe, T., Yamaguchi-Iwai, Y., Sasaki, R. and Nagao, M.** Overview of mammalian zinc transporters. *Cell Mol Life Sci*, 2004, **61**(1), 49-68.
- 10 **Chao, Y. and Fu, D.** Kinetic Study of the Antiport Mechanism of an *Escherichia coli* Zinc Transporter, ZitB. *J Biol Chem*, 2004, **279**(13), 12043-12050.
- 11 **Kawachi, M., Kobae, Y., Mimura, T. and Maeshima, M.** Deletion of a histidine-rich loop of AtMTP1, a vacuolar Zn(2+)/H(+) antiporter of *Arabidopsis thaliana*, stimulates the transport activity. *J Biol Chem*, 2008, **283**(13), 8374-8383.
- 12 **MacDiarmid, C.W., Milanick, M.A. and Eide, D.J.** Biochemical properties of vacuolar zinc transport systems of *Saccharomyces cerevisiae*. *J Biol Chem*, 2002, **277**(42), 39187-39194.
- 13 **Ohana, E., Hoch, E., Keasar, C., Kambe, T., Yifrach, O., Hershfinkel, M. and Sekler, I.** Identification of the Zn²⁺ binding site and mode of operation of a mammalian Zn²⁺ transporter. *J Biol Chem*, 2009, **284**(26), 17677-17686.
- 14 **Anton, A., Grosse, C., Reissmann, J., Pribyl, T. and Nies, D.H.** CzcD is a heavy metal ion transporter involved in regulation of heavy metal resistance in *Ralstonia* sp. strain CH34. *J Bacteriol*, 1999, **181**(22), 6876-6881.
- 15 **Anton, A., Weltrowski, A., Haney, C.J., Franke, S., Grass, G., Rensing, C. and Nies, D.H.** Characteristics of zinc transport by two bacterial cation diffusion facilitators from *Ralstonia metallidurans* CH34 and *Escherichia coli*. *J Bacteriol.*, 2004, **186**(22), 7499-7507.

- 16 Delhaize, E., Kataoka, T., Hebb, D.M., White, R.G. and Ryan, P.R.** Genes encoding proteins of the cation diffusion facilitator family that confer manganese tolerance. *Plant Cell*, 2003, **15**(5), 1131-1142.
- 17 Lin, H., Kumanovics, A., Nelson, J.M., Warner, D.E., Ward, D.M. and Kaplan, J.** A single amino acid change in the yeast vacuolar metal transporters ZRC1 and COT1 alters their substrate specificity. *J Biol Chem*, 2008, **283**(49), 33865-33873.
- 18 Munkelt, D., Grass, G. and Nies, D.H.** The chromosomally encoded cation diffusion facilitator proteins DmeF and FieF from *Wautersia metallidurans* CH34 are transporters of broad metal specificity. *J Bacteriol*, 2004, **186**(23), 8036-8043.
- 19 Persans, M.W., Nieman, K. and Salt, D.E.** Functional activity and role of cation-efflux family members in Ni hyperaccumulation in *Thlaspi goesingense*. *Proc Natl Acad Sci U S A*, 2001, **98**(17), 9995-10000.
- 20 Nies, D.H.** Efflux-mediated heavy metal resistance in prokaryotes. *FEMS Microbiol Rev*, 2003, **27**(2-3), 313-339.
- 21 Spada, S., Pembroke, J.T. and Wall, J.G.** Isolation of a novel *Thermus thermophilus* metal efflux protein that improves *Escherichia coli* growth under stress conditions. *Extremophiles*, 2002, **6**(4), 301-308.
- 22 Conklin, D.S., McMaster, J.A., Culbertson, M.R. and Kung, C.** COT1, a gene involved in cobalt accumulation in *Saccharomyces cerevisiae*. *Mol Cell Biol*, 1992, **12**(9), 3678-3688.
- 23 MacDiarmid, C.W., Milanick, M.A. and Eide, D.J.** Induction of the ZRC1 metal tolerance gene in zinc-limited yeast confers resistance to zinc shock. *J Biol Chem*, 2003, **278**(17), 15065-15072.
- 24 Ellis, C.D., Wang, F., MacDiarmid, C.W., Clark, S., Lyons, T. and Eide, D.J.** Zinc and the Msc2 zinc transporter protein are required for endoplasmic reticulum function. *J Cell Biol*, 2004, **166**(3), 325-335.
- 25 Li, L. and Kaplan, J.** The yeast gene MSC2, a member of the cation diffusion facilitator family, affects the cellular distribution of zinc. *J Biol Chem*, 2001, **276**(7), 5036-5043.
- 26 Li, L. and Kaplan, J.** Characterization of two homologous yeast genes that encode mitochondrial iron transporters. *J Biol Chem*, 1997, **272**(45), 28485-28493.
- 27 Maser, P., Thomine, S., Schroeder, J.I., Ward, J.M., Hirschi, K., Sze, H., Talke, I.N., Amtmann, A., Maathuis, F.J., Sanders, D., Harper, J.F., Tchieu, J., Gribskov, M., Persans, M.W., Salt, D.E., Kim, S.A. and Guerinot, M.L.** Phylogenetic relationships within cation transporter families of *Arabidopsis*. *Plant Physiol*, 2001, **126**(4), 1646-1667.
- 28 Palmer, C.M. and Guerinot, M.L.** Facing the challenges of Cu, Fe and Zn homeostasis in plants. *Nat Chem Biol*, 2009, **5**(5), 333-340.

- 29 **Kobae, Y., Uemura, T., Sato, M.H., Ohnishi, M., Mimura, T., Nakagawa, T. and Maeshima, M.** Zinc transporter of Arabidopsis thaliana AtMTP1 is localized to vacuolar membranes and implicated in zinc homeostasis. *Plant Cell Physiol*, 2004, **45**(12), 1749-1758.
- 30 **Palmiter, R. and Findley, S.** Cloning and functional characterization of a mammalian zinc transporter that confers resistance to zinc. *EMBO Journal*, 1995, **14**(4), 639-649.
- 31 **Cousins, R.J., Liuzzi, J.P. and Lichten, L.A.** Mammalian zinc transport, trafficking, and signals. *J Biol Chem.*, 2006, **281**(34), 24085-24089. .
- 32 **Levy, S., Beharier, O., Etzion, Y., Mor, M., Buzaglo, L., Shaltiel, L., Gheber, L.A., Kahn, J., Muslin, A.J., Katz, A., Gitler, D. and Moran, A.** Molecular basis for zinc transporter 1 action as an endogenous inhibitor of L-type calcium channels. *J Biol Chem*, 2009, **284**(47), 32434-32443.
- 33 **Jirakulaporn, T. and Muslin, A.J.** Cation diffusion facilitator proteins modulate Raf-1 activity. *J Biol Chem*, 2004, **279**(26), 27807-27815.
- 34 **Cole, T.B., Wenzel, H.J., Kafer, K.E., Schwartzkroin, P.A. and Palmiter, R.D.** Elimination of zinc from synaptic vesicles in the intact mouse brain by disruption of the ZnT3 gene. *Proc Natl Acad Sci U S A.*, 1999, **96**(4), 1716-1721.
- 35 **Palmiter, R.D., Cole, T.B., Quaife, C.J. and Findley, S.D.** ZnT-3, a putative transporter of zinc into synaptic vesicles. *Proc Natl Acad Sci U S A*, 1996, **93**(25), 14934-14939.
- 36 **Chimienti, F., Devergnas, S., Pattou, F., Schuit, F., Garcia-Cuenca, R., Vandewalle, B., Kerr-Conte, J., Van Lommel, L., Grunwald, D., Favier, A. and Seve, M.** In vivo expression and functional characterization of the zinc transporter ZnT8 in glucose-induced insulin secretion. *J Cell Sci.*, 2006, **119**(Pt 20), 4199-4206.
- 37 **Sladek, R., Rocheleau, G., Rung, J., Dina, C., Shen, L., Serre, D., Boutin, P., Vincent, D., Belisle, A., Hadjadj, S., Balkau, B., Heude, B., Charpentier, G., Hudson, T.J., Montpetit, A. and et al.** A genome-wide association study identifies novel risk loci for type 2 diabetes. *Nature.*, 2007, **445**(7130), 881-885.
- 38 **Lemaire, K., Ravier, M.A., Schraenen, A., Creemers, J.W., Van de Plas, R., Granvik, M., Van Lommel, L., Waelkens, E., Chimienti, F., Rutter, G.A., Gilon, P., in't Veld, P.A. and Schuit, F.C.** Insulin crystallization depends on zinc transporter ZnT8 expression, but is not required for normal glucose homeostasis in mice. *Proc Natl Acad Sci U S A*, 2009, **106**(35), 14872-14877.
- 39 **Studier, F.W. and Moffatt, B.A.** Use of bacteriophage T7 RNA polymerase to direct selective high-level expression of cloned genes. *J Mol Biol*, 1986, **189**(1), 113-130.
- 40 **Studier, F.W.** Protein production by auto-induction in high density shaking cultures. *Protein Expr Purif.*, 2005, **41**(1), 207-234.

- 41 **Chao, Y. and Fu, D.** Thermodynamic studies of the mechanism of metal binding to the Escherichia coli zinc transporter YjiP. *J Biol Chem*, 2004, **279**(17), 17173-17180.
- 42 **Hayashi, Y., Matsui, H. and Takagi, T.** Membrane protein molecular weight determined by low-angle laser light-scattering photometry coupled with high-performance gel chromatography. *Methods Enzymol*, 1989, **172**, 514-528.
- 43 **Wei, Y., Li, H. and Fu, D.** Oligomeric state of the Escherichia coli metal transporter YjiP. *J. Biol. Chem.*, 2004, **279**, 39251-39259.
- 44 **Lu, M. and Fu, D.** Structure of the zinc transporter YjiP. *Science.*, 2007, **317**(5845), 1746-1748. .
- 45 **Lu, M., Chai, J. and Fu, D.** Structural basis for autoregulation of the zinc transporter YjiP. *Nat Struct Mol Biol*, 2009, **16**(10), 1063-1067.
- 46 **Cherezov, V., Rosenbaum, D.M., Hanson, M.A., Rasmussen, S.G., Thian, F.S., Kobilka, T.S., Choi, H.J., Kuhn, P., Weis, W.I., Kobilka, B.K. and Stevens, R.C.** High-resolution crystal structure of an engineered human beta2-adrenergic G protein-coupled receptor. *Science*, 2007, **318**(5854), 1258-1265.
- 47 **Pebay-Peyroula, E., Rummel, G., Rosenbusch, J.P. and Landau, E.M.** X-ray structure of bacteriorhodopsin at 2.5 angstroms from microcrystals grown in lipidic cubic phases. *Science*, 1997, **277**(5332), 1676-1681.
- 48 **Rasmussen, S.G., Choi, H.J., Rosenbaum, D.M., Kobilka, T.S., Thian, F.S., Edwards, P.C., Burghammer, M., Ratnala, V.R., Sanishvili, R., Fischetti, R.F., Schertler, G.F., Weis, W.I. and Kobilka, B.K.** Crystal structure of the human beta2 adrenergic G-protein-coupled receptor. *Nature*, 2007, **450**(7168), 383-387.
- 49 **Abramson, J., Smirnova, I., Kasho, V., Verner, G., Kaback, H.R. and Iwata, S.** Structure and mechanism of the lactose permease of Escherichia coli. *Science*, 2003, **301**(5633), 610-615.
- 50 **Mirza, O., Guan, L., Verner, G., Iwata, S. and Kaback, H.R.** Structural evidence for induced fit and a mechanism for sugar/H⁺ symport in LacY. *EMBO J*, 2006, **25**(6), 1177-1183.
- 51 **Yao, X., Parnot, C., Deupi, X., Ratnala, V.R., Swaminath, G., Farrens, D. and Kobilka, B.** Coupling ligand structure to specific conformational switches in the beta2-adrenoceptor. *Nat Chem Biol*, 2006, **2**(8), 417-422.
- 52 **Yin, Y., Jensen, M.O., Tajkhorshid, E. and Schulten, K.** Sugar binding and protein conformational changes in lactose permease. *Biophys J*, 2006, **91**(11), 3972-3985.
- 53 **Wernimont, A.K., Huffman, D.L., Lamb, A.L., O'Halloran, T.V. and Rosenzweig, A.C.** Structural basis for copper transfer by the metallochaperone for the Menkes/Wilson disease proteins. *Nat Struct Biol.*, 2000, **7**(9), 766-771.

- 54 Finney, L.A. and O'Halloran, T.V.** Transition metal speciation in the cell: insights from the chemistry of metal ion receptors. *Science.*, 2003, **300**(5621), 931-936.
- 55 Huang, Y., Lemieux, M.J., Song, J., Auer, M. and Wang, D.N.** Structure and mechanism of the glycerol-3-phosphate transporter from *Escherichia coli*. *Science*, 2003, **301**(5633), 616-620.
- 56 Hunte, C., Screpanti, E., Venturi, M., Rimon, A., Padan, E. and Michel, H.** Structure of a Na⁺/H⁺ antiporter and insights into mechanism of action and regulation by pH. *Nature.*, 2005, **435**(7046), 1197-1202.
- 57 Yamashita, A., Singh, S.K., Kawate, T., Jin, Y. and Gouaux, E.** Crystal structure of a bacterial homologue of Na⁺/Cl⁻-dependent neurotransmitter transporters. *Nature.*, 2005, **437**(7056), 215-223.
- 58 Hilgemann, D.W.** Regulation and deregulation of cardiac Na⁽⁺⁾-Ca²⁺ exchange in giant excised sarcolemmal membrane patches. *Nature.*, 1990, **344**(6263), 242-245.
- 59 Besserer, G.M., Ottolia, M., Nicoll, D.A., Chaptal, V., Cascio, D., Philipson, K.D. and Abramson, J.** The second Ca²⁺-binding domain of the Na⁺ Ca²⁺ exchanger is essential for regulation: crystal structures and mutational analysis. *Proc Natl Acad Sci U S A.*, 2007, **104**(47), 18467-18472.
- 60 Eshaghi, S., Niegowski, D., Kohl, A., Martinez Molina, D., Lesley, S.A. and Nordlund, P.** Crystal structure of a divalent metal ion transporter CorA at 2.9 angstrom resolution. *Science.*, 2006, **313**(5785), 354-357.
- 61 Hattori, M., Tanaka, Y., Fukai, S., Ishitani, R. and Nureki, O.** Crystal structure of the MgtE Mg²⁺ transporter. *Nature.*, 2007, **448**(7157), 1072-1075.
- 62 Lunin, V.V., Dobrovetsky, E., Khutoreskaya, G., Zhang, R., Joachimiak, A., Doyle, D.A., Bochkarev, A., Maguire, M.E., Edwards, A.M. and Koth, C.M.** Crystal structure of the CorA Mg²⁺ transporter. *Nature.*, 2006, **440**(7085), 833-837.
- 63 Payandeh, J. and Pai, E.F.** A structural basis for Mg²⁺ homeostasis and the CorA translocation cycle. *EMBO J*, 2006, **25**(16), 3762-3773.
- 64 Hilge, M., Aelen, J. and Vuister, G.W.** Ca²⁺ regulation in the Na⁺/Ca²⁺ exchanger involves two markedly different Ca²⁺ sensors. *Mol Cell.*, 2006, **22**(1), 15-25.
- 65 Nies, D.H.** Biochemistry. How cells control zinc homeostasis. *Science.*, 2007, **317**(5845), 1695-1696.
- 66 Frausto da Silva, J. and Williams, R.** *The biological chemistry of the elements-The inorganic chemistry of life.* (Oxford University Press, 2001).
- 67 Maret, W. and Li, Y.** Coordination dynamics of zinc in proteins. *Chem Rev*, 2009, **109**(10), 4682-4707.

- 68 Sousa, S.F., Fernandes, P.A. and Ramos, M.J.** The carboxylate shift in zinc enzymes: a computational study. *J Am Chem Soc.*, 2007, **129**(5), 1378-1385.
- 69 Vallee, B.L. and Auld, D.S.** Active-site zinc ligands and activated H₂O of zinc enzymes. *Proc Natl Acad Sci U S A.*, 1990, **87**(1), 220-224.
- 70 Wei, Y. and Fu, D.** Binding and transport of metal ions at the dimer interface of the Escherichia coli metal transporter YiiP. *J Biol Chem.*, 2006, **281**(33), 23492-23502.
- 71 Doyle, D.A., Morais Cabral, J., Pfuetzner, R.A., Kuo, A., Gulbis, J.M., Cohen, S.L., Chait, B.T. and MacKinnon, R.** The structure of the potassium channel: molecular basis of K⁺ conduction and selectivity. *Science.*, 1998, **280**(5360), 69-77.
- 72 Padan, E. and Schuldiner, S.** Intracellular pH and membrane potential as regulators in the prokaryotic cell. *J Membr Biol*, 1987, **95**(3), 189-198.
- 73 Luecke, H., Richter, H.T. and Lanyi, J.K.** Proton transfer pathways in bacteriorhodopsin at 2.3 angstrom resolution. *Science.*, 1998, **280**(5371), 1934-1937.
- 74 Di Costanzo, L., Flores, L.V., Jr. and Christianson, D.W.** Stereochemistry of guanidine-metal interactions: implications for L-arginine-metal interactions in protein structure and function. *Proteins.*, 2006, **65**(3), 637-642.
- 75 Cherezov, V., Hofer, N., Szebenyi, D.M., Kolaj, O., Wall, J.G., Gillilan, R., Srinivasan, V., Jaroniec, C.P. and Caffrey, M.** Insights into the mode of action of a putative zinc transporter CzcB in *Thermus thermophilus*. *Structure.*, 2008, **16**(9), 1378-1388.
- 76 Rosenzweig, A.C. and O'Halloran, T.V.** Structure and chemistry of the copper chaperone proteins. *Curr Opin Chem Biol.*, 2000, **4**(2), 140-147.
- 77 Huffman, D.L. and O'Halloran, T.V.** Function, structure, and mechanism of intracellular copper trafficking proteins. *Annu Rev Biochem*, 2001, **70**, 677-701.
- 78 Arnesano, F., Banci, L., Bertini, I., Ciofi-Baffoni, S., Molteni, E., Huffman, D.L. and O'Halloran, T.V.** Metallochaperones and metal-transporting ATPases: a comparative analysis of sequences and structures. *Genome Res*, 2002, **12**(2), 255-271.
- 79 Klomp, L.W., Lin, S.J., Yuan, D.S., Klausner, R.D., Culotta, V.C. and Gitlin, J.D.** Identification and functional expression of HAH1, a novel human gene involved in copper homeostasis. *J Biol Chem*, 1997, **272**(14), 9221-9226.
- 80 Harris, E.D.** Cellular copper transport and metabolism. *Annu Rev Nutr*, 2000, **20**, 291-310.
- 81 Cox, D.W. and Moore, S.D.** Copper transporting P-type ATPases and human disease. *J Bioenerg Biomembr*, 2002, **34**(5), 333-338.

- 82 Lutsenko, S., Efremov, R.G., Tsivkovskii, R. and Walker, J.M.** Human copper-transporting ATPase ATP7B (the Wilson's disease protein): biochemical properties and regulation. *J Bioenerg Biomembr*, 2002, **34**(5), 351-362.
- 83 Achila, D., Banci, L., Bertini, I., Bunce, J., Ciofi-Baffoni, S. and Huffman, D.L.** Structure of human Wilson protein domains 5 and 6 and their interplay with domain 4 and the copper chaperone HAH1 in copper uptake. *Proc Natl Acad Sci U S A*, 2006, **103**(15), 5729-5734.
- 84 Yatsunyk, L.A. and Rosenzweig, A.C.** Cu(I) binding and transfer by the N terminus of the Wilson disease protein. *J Biol Chem*, 2007, **282**(12), 8622-8631.
- 85 Pufahl, R.A., Singer, C.P., Peariso, K.L., Lin, S.J., Schmidt, P.J., Fahrni, C.J., Culotta, V.C., Penner-Hahn, J.E. and O'Halloran, T.V.** Metal ion chaperone function of the soluble Cu(I) receptor Atx1. *Science*, 1997, **278**(5339), 853-856.
- 86 Rensing, C., Fan, B., Sharma, R., Mitra, B. and Rosen, B.P.** CopA: An Escherichia coli Cu(I)-translocating P-type ATPase. *Proc Natl Acad Sci U S A*, 2000, **97**(2), 652-656.
- 87 Rensing, C., Mitra, B. and Rosen, B.P.** The zntA gene of Escherichia coli encodes a Zn(II)-translocating P-type ATPase. *Proc Natl Acad Sci U S A*, 1997, **94**(26), 14326-14331.
- 88 Banci, L., Bertini, I., Ciofi-Baffoni, S., Finney, L.A., Outten, C.E. and O'Halloran, T.V.** A new zinc-protein coordination site in intracellular metal trafficking: solution structure of the Apo and Zn(II) forms of ZntA(46-118). *J Mol Biol.*, 2002, **323**(5), 883-897.

FIGURE LEGENDS

Figure 1 Schematic representation of the homodimer structure of YiiP. The transmembrane domain (TMD) is colored in cyan, the C-terminal domain (CTD) in green, and zinc atoms in magenta. PDB code: 3H90. Prepared with the program PyMol (<http://www.pymol.org/>)

Figure 2 Topology diagram of a YiiP protomer. α -helices and β -strands are represented by cylinders and arrows, respectively. The labelling of the secondary structure elements is adopted from reference 44. Note, SA is the active site for zinc transport.

Figure 3 Cross-section of a YiiP homodimer viewed from the membrane plane. One protomer is shown in ribbon representation, and the other in solvent-accessible surface with TM1 and TM2 removed to reveal the sequestered TM5 (yellow patch) and a bound zinc ion

(magenta sphere) at the bottom of the extracellular cavity. Solid lines depict the membrane boundaries, dashed lines outline the cavity boundaries and arrows indicate the openings of the extracellular and intracellular cavity, respectively.

Figure 4 Drawing of the active-site (SA) for zinc transport with bound distances as indicated.

Figure 5 Drawing of the zinc binding site (SB) on the cytoplasmic membrane surface with bound distances as indicated.

Figure 6 Drawing of the binuclear zinc binding site (SC) at the CTD-CTD interface.

Figure 7 Proposal for the $\text{Zn}^{2+}/\text{H}^{+}$ antiport mechanism

Figure 8 Schematic drawing of the proposed zinc-regulated zinc transport mechanism. Note, the red-cross at the conjuncture between TMD and CTD represents the charge interlock located at the pivotal point of a hinge-like motion.

Figure 9 Proposed mechanism of Zn^{2+} uploading into the intracellular cavity from a putative Zn^{2+} -metallochaperone. (A) Superposition of a CTD and a Hah1 protomer. The CDT and Hah1 homodimers are colored in green and magenta, respectively. The orange sphere represents a Cd^{2+} located at the metal transfer site of a Hah1 homodimer. PDB code: 1FE0. (B) Docking of Hah1 onto YiiP shown in molecular surface representation.

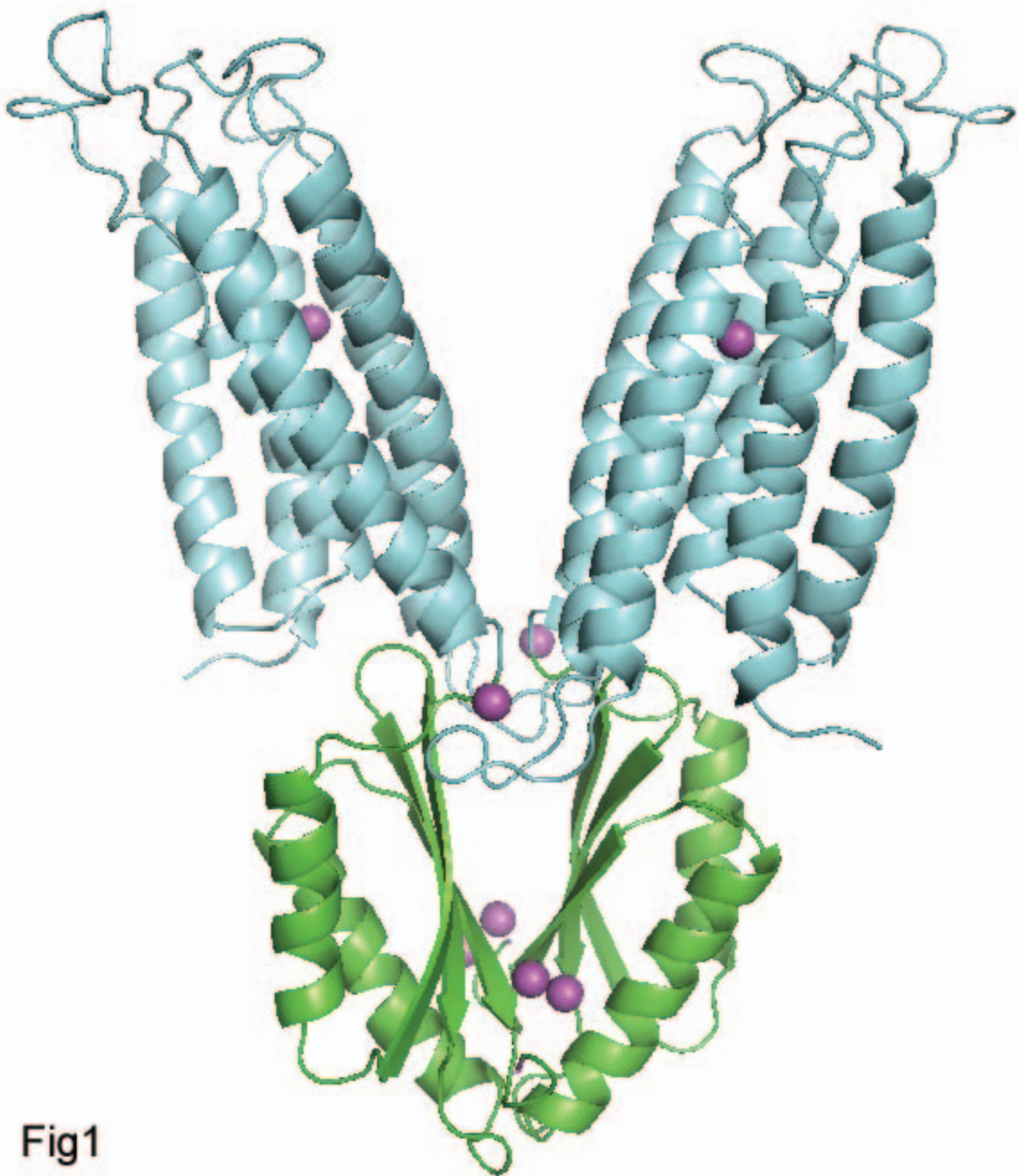


Fig1

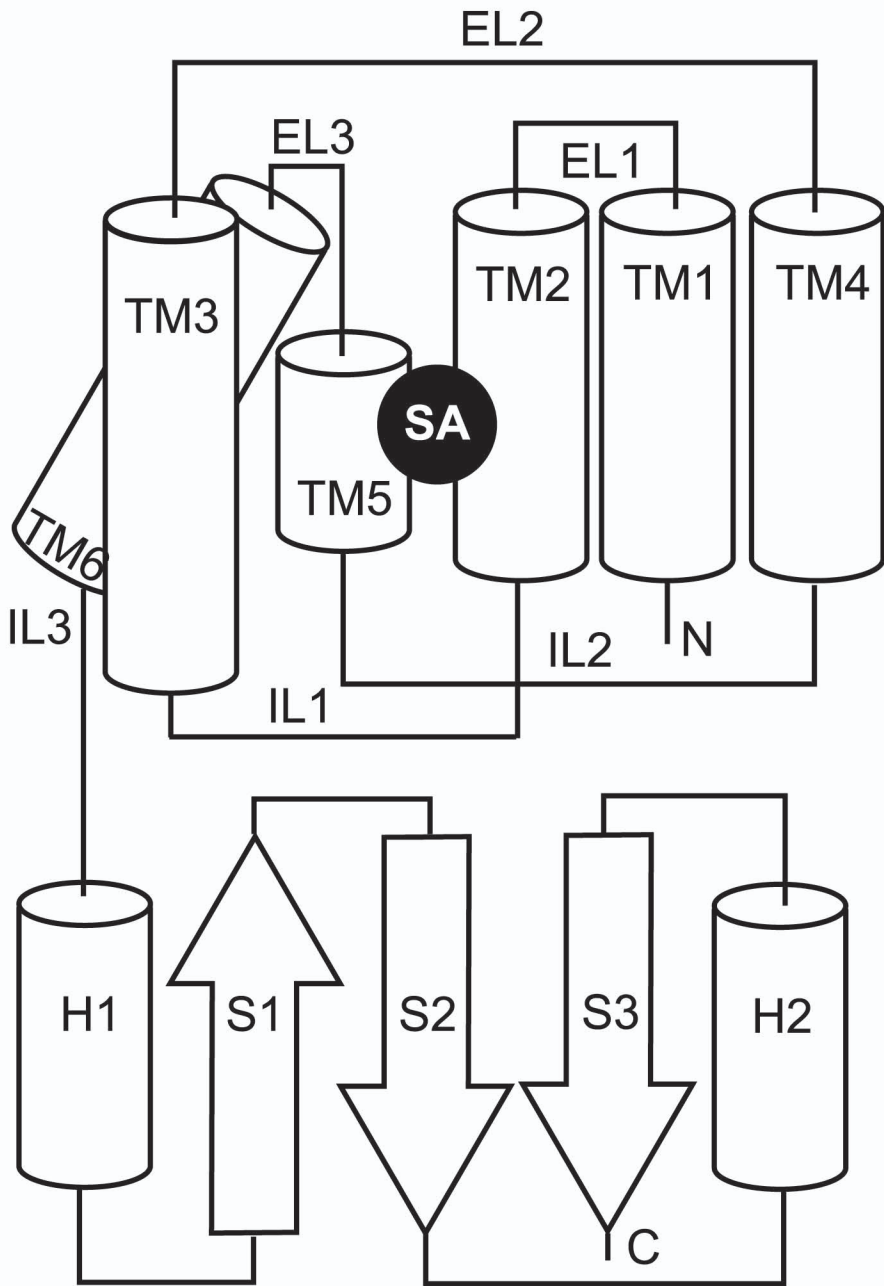


Fig2

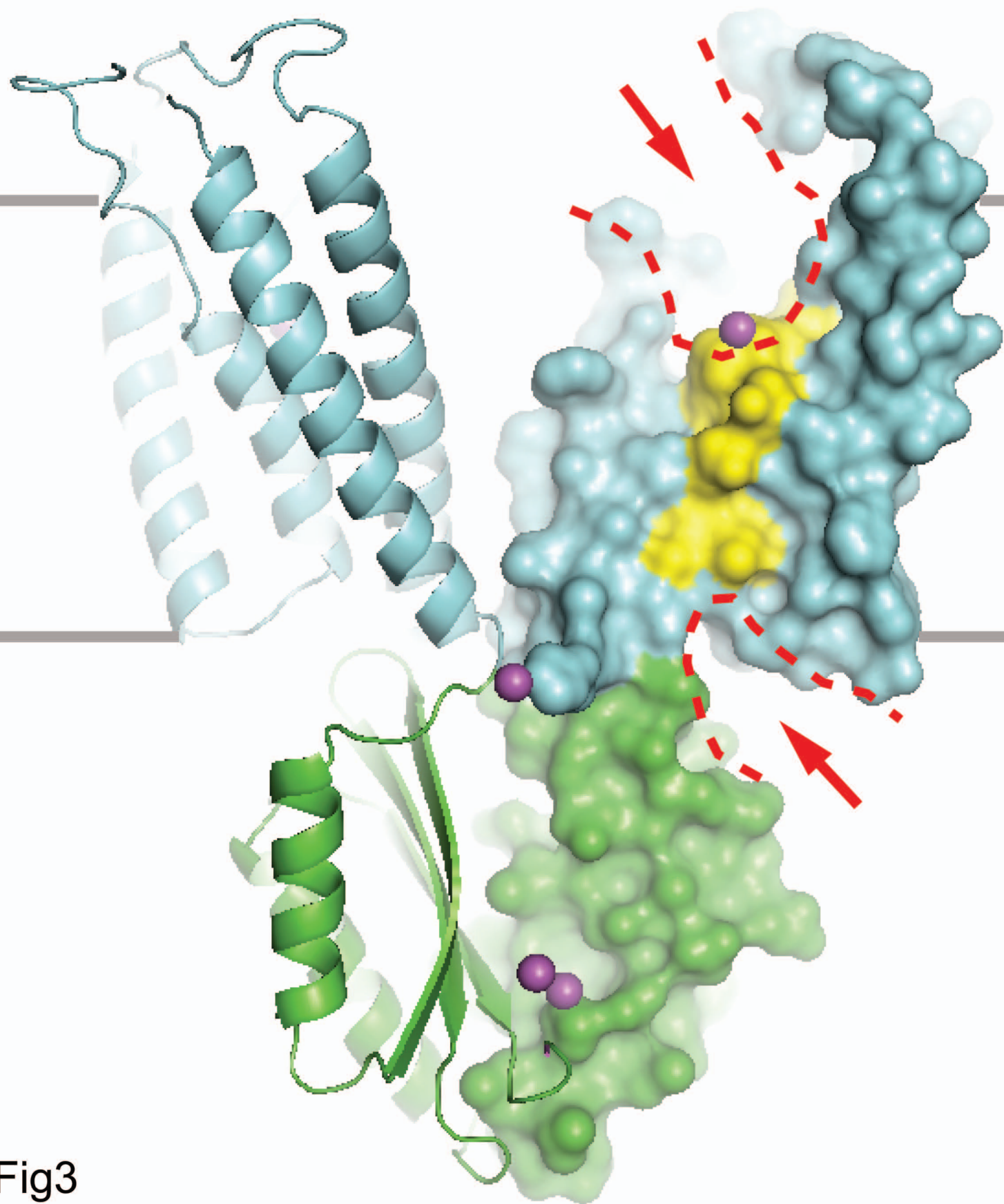


Fig3

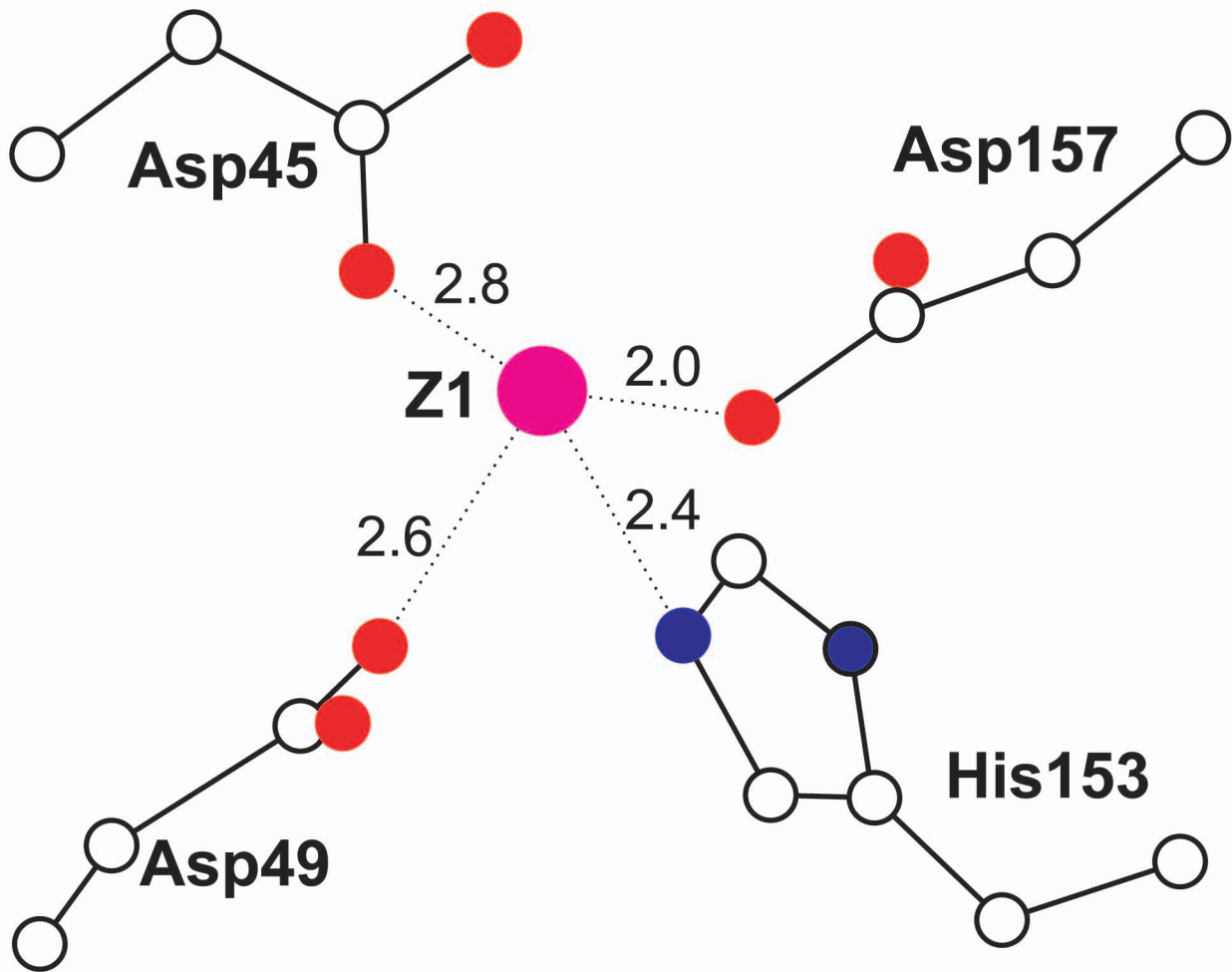


Fig4

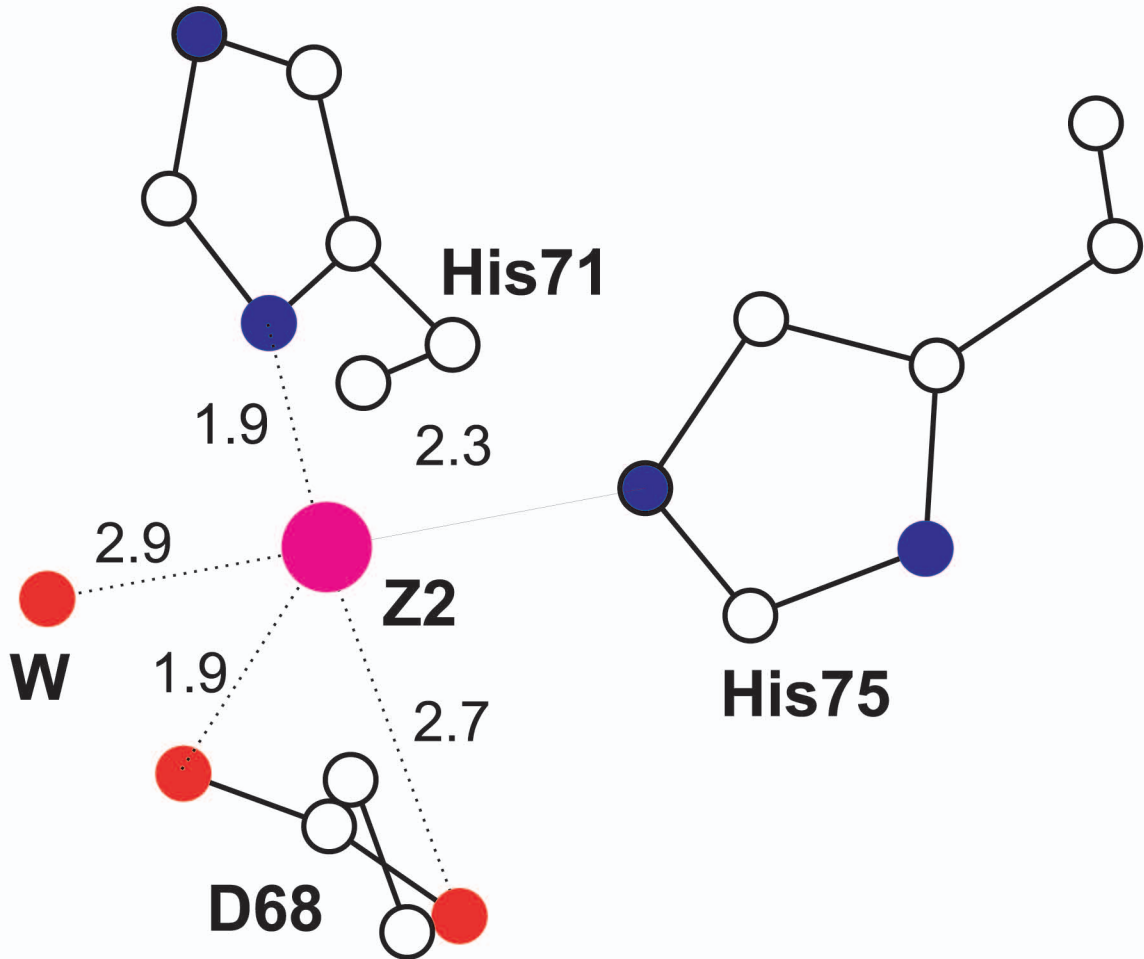


Fig5

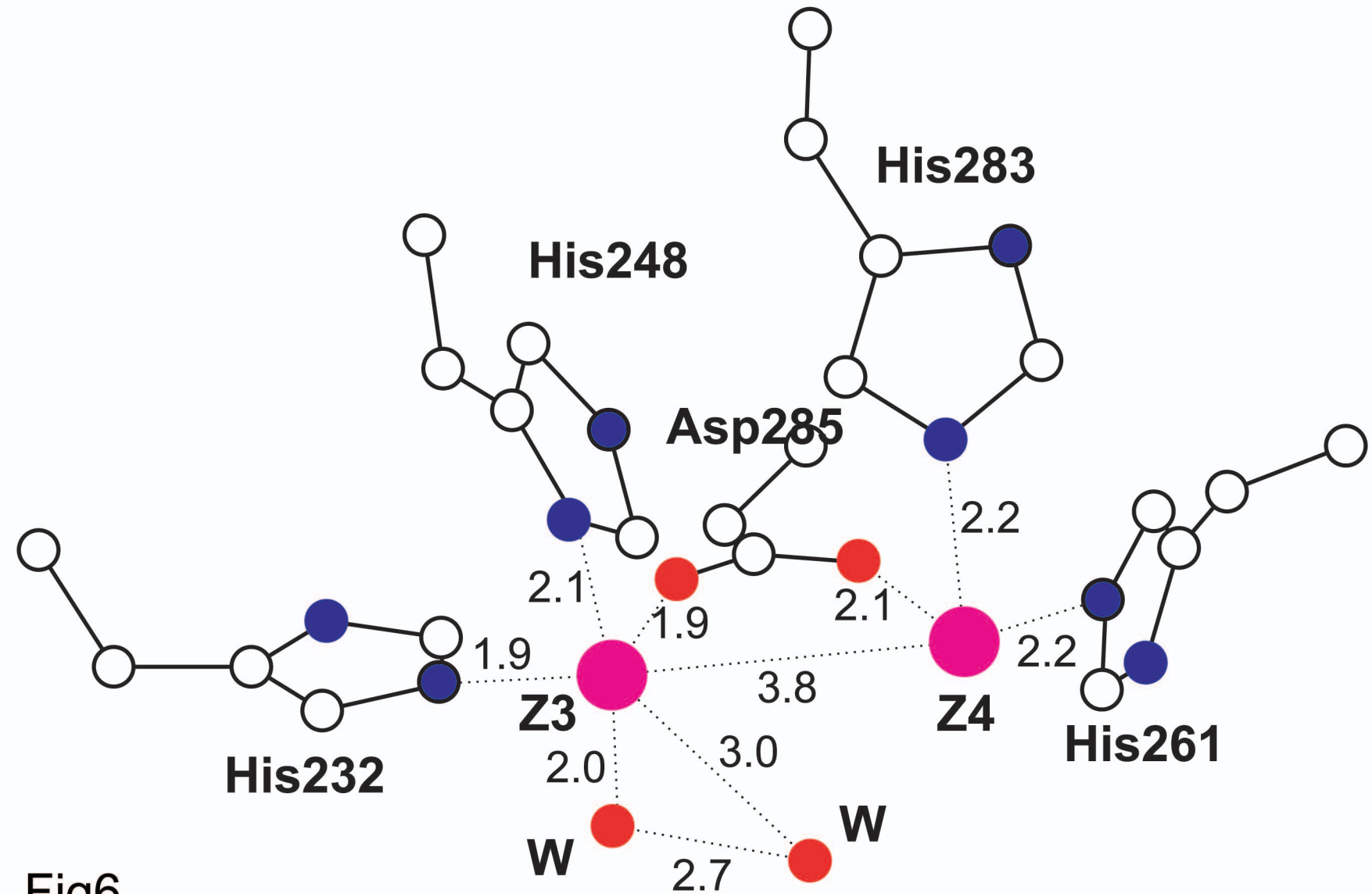


Fig6

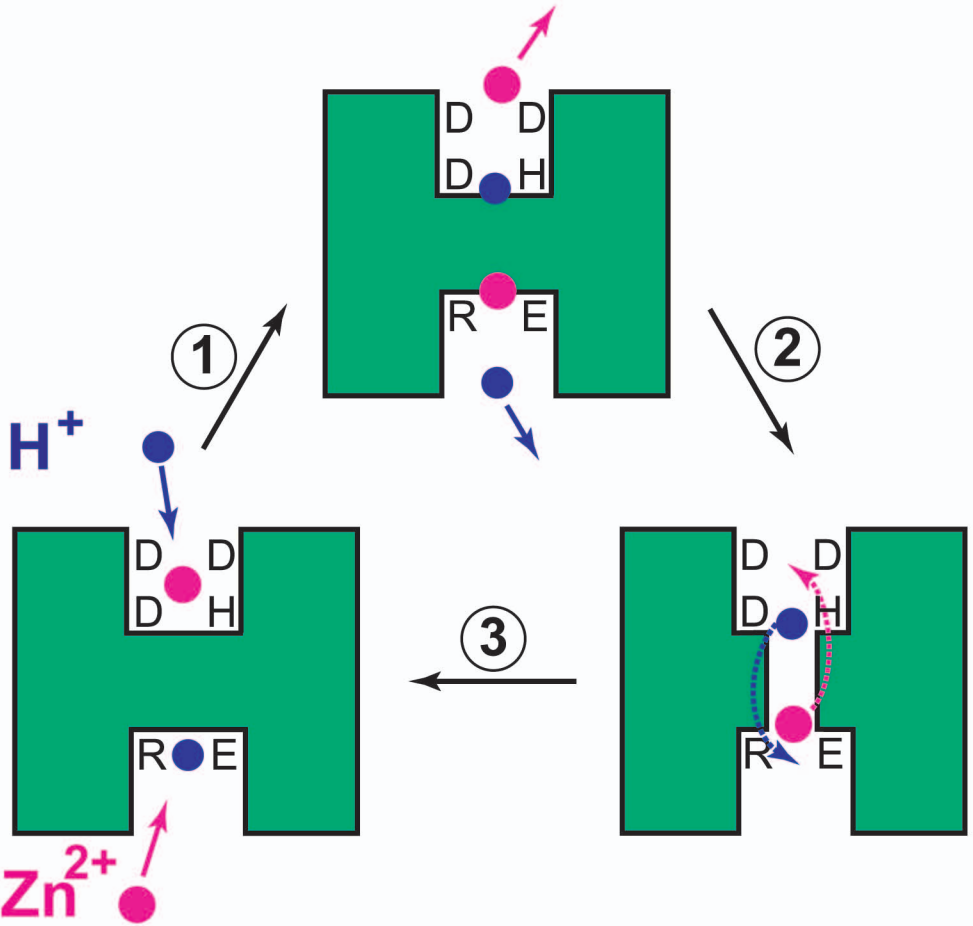


Fig7

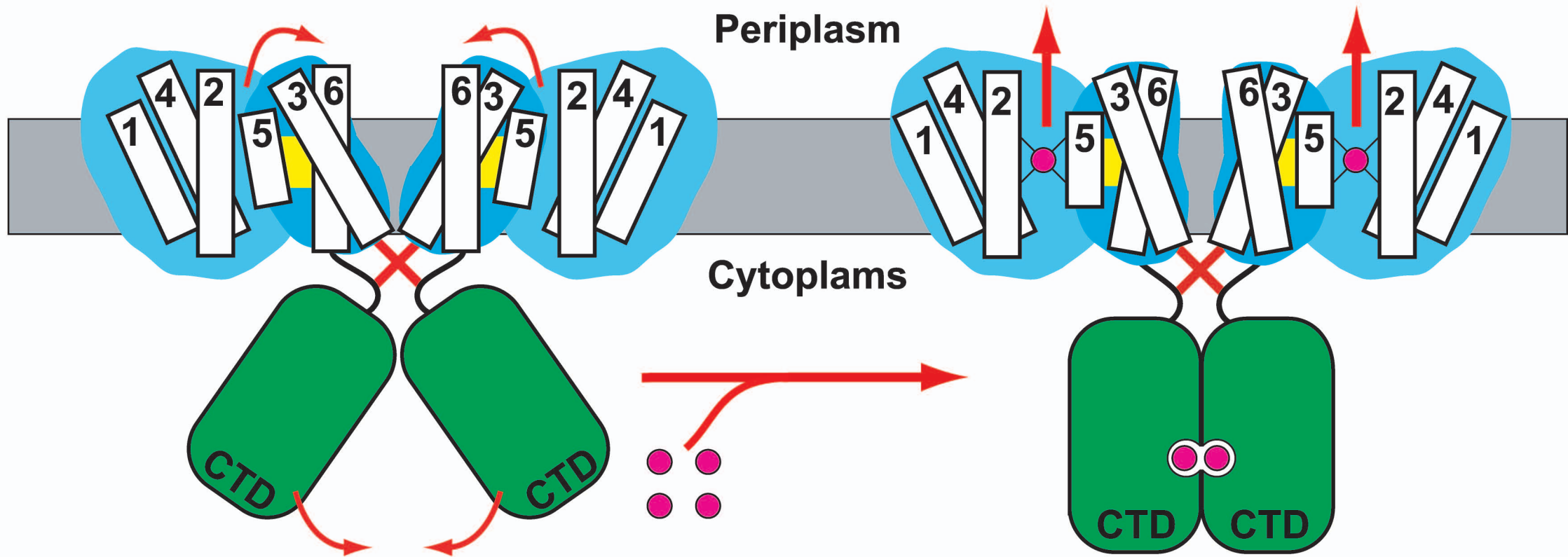


Fig8

A



B

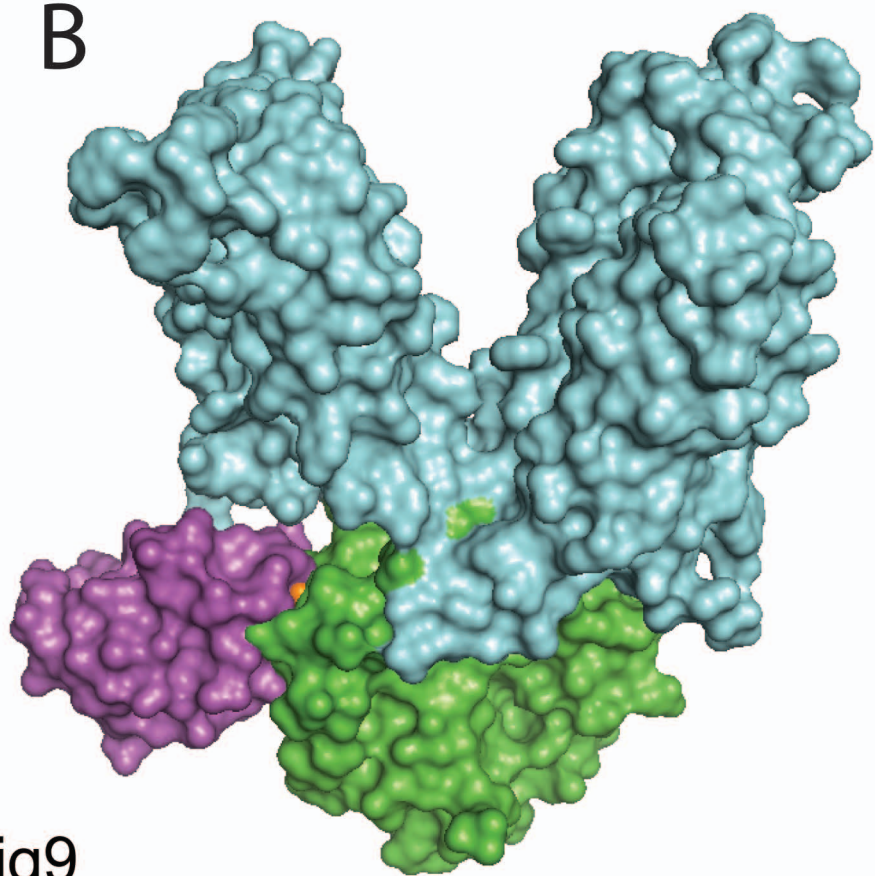


Fig9